

Article

Suppression of Hydrophobic Recovery in Photo-Initiated Chemical Vapor Deposition

Alessio Aufoujal¹, Ulrich Legrand¹, Jean-Luc Meunier² and Jason Robert Tavares^{1,*} 

¹ Research Center for High Performance Polymer and Composite Systems (CREPEC), Department of Chemical Engineering Department, Polytechnique Montreal, Montreal, QC H3C 3A7, Canada; alessio.aufoujal@polymtl.ca (A.A.); ulrich.legrand@polymtl.ca (U.L.)

² Plasma Processing Laboratory, Department of Chemical Engineering, McGill University, Montreal, QC H3A 2B2, Canada; jean.luc.meunier@mcgill.ca

* Correspondence: jason.tavares@polymtl.ca; Tel.: +1-514-340-4711 (ext. 2326)

Received: 9 April 2020; Accepted: 11 May 2020; Published: 12 May 2020



Abstract: Photo-initiated chemical vapor deposition (PICVD) functionalizes carbon nanotube (CNT)-enhanced porous substrates with a highly polar polymeric nanometric film, rendering them super-hydrophilic. Despite its ability to generate fully wettable surfaces at low temperatures and atmospheric pressure, PICVD coatings normally undergo hydrophobic recovery. This is a process by which a percentage of oxygenated functional group diffuse/re-arrange from the top layer of the deposited film towards the bulk of the substrate, taking the induced hydrophilic property of the material with them. Thus, hydrophilicity decreases over time. To address this, a vertical chemical gradient (VCG) can be deposited onto the CNT-substrate. The VCG consists of a first, thicker highly cross-linked layer followed by a second, thinner highly functionalized layer. In this article, we show, through water contact angle and XPS measurements, that the increased cross-linking density of the first layer can reduce the mobility of polar functional groups, forcing them to remain at the topmost layer of the PICVD coating and to suppress hydrophobic recovery. We show that employing a bi-layer VCG suppresses hydrophobic recovery for five days and reduces its effect afterwards (contact angle stabilizes to $42 \pm 1^\circ$ instead of $125 \pm 3^\circ$).

Keywords: hydrophobic recovery; photochemistry; superhydrophilicity; homogenous catalysis

1. Introduction

Special wettability surfaces such as superhydrophobic, superhydrophilic, and heterogeneous or patterned wettabilities have gained significant interest since the development of surface modification techniques [1–5]. Patterned wettability research has focused on combining both superhydrophobicity and superhydrophilicity on a single surface such that it can benefit from both the repellent and spreading properties of each. This can be done two-dimensionally by creating patterns such as lines or shapes on a given substrate that express the opposite behavior to the remaining, untreated part of the surface. Yu et al. showed an example of this by first spraying a superhydrophobic coating of silica poly(dimethyl siloxane) (PDMS) onto a substrate, thus creating a hydrophobic background [6]. Then, a superhydrophilic layer of platinum (Pt) was deposited via pulsed laser deposition (PLD) using a grid mask. This yielded patterned wettability surfaces that had a hydrophilic background with hydrophobic micro bumps, mimicking the shell of *Stenocara gracilipes*, a beetle that uses this surface texture to capture fog from the atmosphere [6]. Superhydrophilic surfaces on their own have also gained industrial interest for their anti-fogging, microfluidic, and heat transfer applications [5]. Another important application for superhydrophilic surfaces lies in their anti-fouling properties. Though the mechanism behind biofouling formation is a complex process, it has been demonstrated that overall

fouling decreases with high surface energy surfaces, a relationship that is associated with hydrophilic behavior. A high affinity between surface and water molecules generates films on these surfaces [2,7,8]. Hence, interactions between fouling agents and the surface are limited. One major drawback for this process is the low stability of such superhydrophilic surfaces, reducing fouling prevention in the long-term. As an example, fouling has been linked to marine applications such as the growth of microorganisms on the submerged surface of ships. Current remediation techniques include the use of biocides. However, this type of substance causes environmental damage [9,10].

Generally, extreme wettability features can be achieved through the modification of surface topology, tailoring the surface chemistry of a material or a combination of both topological and chemical techniques [11,12]. Superhydrophilic surfaces obtained via chemical approaches suffer from a key drawback: in many cases, artificially-induced superhydrophilic surfaces lose their wettability over time due to a phenomenon known as hydrophobic recovery [13–17]. This process can occur as soon as minutes or hours [18]. This has been extensively observed for plasma-modified polymers and plasma polymer films (PPF) [19–23]. Hydrophobic recovery has been linked to different mechanisms:

- (1) Rearrangement and reorientation of polar functional groups at the surface [13–15,24];
- (2) Diffusion of the low molecular weight chemical groups from the outer surface towards the bulk of the deposited polymer [20,25,26];
- (3) Oxidation and degradation reactions occurring at the surface over time [20,25,26];
- (4) Surface roughness changes or adventitious external contamination [14,27,28].

These mechanisms can co-exist within a single polymer layer and are mostly dependent on material properties such as the mobility of the polymer chain, the degree of cross-linking of the polymer structure, the chemical composition of the polymer, and any additives that may be present. External factors such as the polarity, temperature, and pressure of the storage environment of the samples also influence hydrophobic recovery [19–21,29,30]. Polymeric molecules in a thin layer have a degree of freedom to move and may change conformations at the interface with another medium to reduce their interfacial energy. The polarity of the outer medium has been found to dictate surface reorganization. In water, a surface tends to expose its polar components and push their non-polar ones into the bulk of the polymer. The inverse scenario has been observed in the case of storage in air. This conclusion has been found on several polymers such as polyethylene (PE), poly(ethylene terephthalate) (PET), and silicon rubber [14,31,32].

A technique that has been shown to reduce hydrophobic recovery in PPF is the use of vertical chemical gradients (VCG) [21–23]. Specifically, Hegemann et al. designed PPFs that possess vertical chemical gradients such that a highly-functional film layer is deposited over a stable, less-functional one [23]. The purpose of the first layer is to prevent both the reorientation of functional polymer chains at the surface and the diffusion of polar functional groups towards the bulk of the substrate. This was done using a capacitively coupled plasma reactor with an ethylene (C_2H_4) and carbon dioxide (CO_2) precursor mixture. By varying this gas ratio, they obtained the desired double layered thin PPF [23,33]. Similarly, Li et al. deposited a bilayer of plasma polymerized heptylamine (PPHA) [34]. In this case, they combined two plasma polymerization modes, continuous and pulsed, to obtain cross-linking in one layer and functionality in the second, respectively. Though the results achieved through these methods have been promising, the scalability and energy intensity of plasma processing can hinder further development towards the application of stable hydrophilic thin films. Building on this past work done in the field of plasma science, we thus turned to the usage of low-cost and sustainable ultraviolet (UV) radiation, a key component leading to reactions in plasma. UV exposure usually photodegrades polymers, observable through the loss of color and the embrittlement of the material [35]. This irradiation causes polymer chain scission and reorganization in the form of the cross-linking of polymer chains. These chemical cross-links effectively reduce the flexibility of a polymer molecule, stiffening the structure, reducing the polymer chain mobility, and ultimately limiting the mobility of smaller molecules [36,37]. We employed this relationship using a chemical vapor

deposition (CVD) gas phase technique that uses UVC light (ultraviolet C subtype, with wavelengths between 200 and 280 nm) to initiate the free radical polymerization of photoactive monomers using a gas-phase homogeneous photocatalyst. Compared to plasma-enhanced or thermally activated CVD, this photo-initiated CVD (PICVD) is performed at atmospheric temperature and pressure, thus greatly reducing processing cost and energy usage and increasing the scalability and sustainability of the technique [38]. Typically, PICVD requires a careful selection of an initial reaction mixture based on its capacity to polymerize onto a substrate, either through self-polymerization or with the help of photo-initiators [39–42]. The selection of monomer precursors depends on the desired properties of the produced thin films. Examples of such monomers include styrene, vinyl esters, vinyl ethers, acrylics, and methacrylates [39,42,43]. These monomers have been as precursors for the synthesis of a variety of polymeric films such as poly(2-hydroxyethyl methacrylate) (pHEMA), poly(methyl methacrylate) (PMMA), polydivinylbenzene (PDVB), and poly(glycidol methacrylate) (PGMA) [39,40,42]. In this work, the precursors consisted of a syngas mixture of carbon monoxide (CO), hydrogen (H₂), a photo initiator, hydrogen peroxide (H₂O₂), and trace amounts of iron pentacarbonyl (Fe(CO)₅). Iron pentacarbonyl was formed in trace quantities (0.02–6.7 ppm) from the reaction of CO and the steel walls of its storage cylinder, and it served as a homogeneous photocatalyst [44]. Through photo-initiated reactions within the gas mixture, a thin oligomeric film was formed on the substrate surface.

Inspired by current advances in reducing hydrophobic recovery in plasma processes, we imposed a VCG by which a highly cross-linked layer is first deposited onto a carbon nanotube forest grown on stainless steel grids (SS-CNT) followed by a second, highly functional layer. CNTs were selected because prior research has demonstrated that they can be readily be functionalized over a wide range of surface energies using PICVD [45]. This work aimed to demonstrate a simple method for increasing stability in superhydrophilic thin films. This novel approach was deemed of interest due to the simplicity of the technique when compared to plasma processing or solvent based ones. PICVD uses common and accessible materials (CO, H₂, and H₂O₂), as well as low energy UVC lamps to perform surface treatments and, in the case of this study, to suppress the effects of aging on superhydrophilic samples—which is in itself an issue that has been encountered by many in the literature. This makes this technique highly scalable. Furthermore, superhydrophilicity is shown here to be maintained over increased time scales. Achieving stable superhydrophilic coatings in this fashion can prove to be beneficial for the previously described industrial purposes. Typically, hydrophobic recovery occurs within a short time frame from hours to days. In this work, we propose a strategy and insight that drastically improve stability in superhydrophilic thin films. To the best of our knowledge, VCG has never been shown in thin film deposition techniques other than capacitively coupled plasma polymerization. In this research article, a vertical chemical gradient strategy employing PICVD films to reduce the effects of hydrophobic recovery on SS-CNT substrates is described.

2. Results

2.1. Surface Modification

Previous work on functionalization via PICVD has shown that a full range of surface wettabilities, from superhydrophilic to superhydrophobic, can be achieved by modifying process parameters such as pressure, gas volume ratio (H₂/CO), sample position, and photo-initiator flow rate [38,45,46]. The effects of these parameters on the wettability of the deposited polymer film are summarized in Table 1.

Table 1. Photo-initiated chemical vapor deposition (PICVD) processing parameters effects on surface wettability.

Process Parameter	Effect on Wettability
Pressure (P)	Increase in pressure decreases wettability ($\theta \propto P$) [45]
Photo-initiator (n_{PI})	Presence of a number density of photo-initiator increases wettability ($\theta \propto \frac{1}{n_{PI}}$) [45]
Position (x)	Wettability is increased when the sample position is near the reactor inlet ($\theta \propto x_{inlet}$) [45,46]
Treatment duration (t)	Increase in treatment duration decreases wettability ($\theta \propto \frac{1}{t}$) [45]
Gas Ratio (R)	Increase in gas ratio decreases wettability ($\theta \propto R$) [45]

From these relationships, processing parameters were selected to achieve hydrophobic, superhydrophilic, and VCG depositions (Table 2). The concept of VCG has already been explored in the context of plasma polymerization and, to translate this approach to a PICVD context, we first deposited a thicker hydrophobic layer for 120 min. Through x-ray photoelectron spectroscopy (XPS) and time-of-flight secondary ion mass spectrometry (TOF-SIMS), previous studies have demonstrated that this polymeric film chemically resembles phenol formaldehyde resin, with a highly cross-linked structure [47]. For the following 60 min, PICVD parameters were changed by decreasing the pressure to 15 kPa and adding hydrogen peroxide (H_2O_2) at a flow rate of 1 mL/min. These conditions corresponded to a hydrophilic treatment and were meant to incorporate oxygenated functional groups in the top-most layer of the polymer film. A schematic of the VCG procedure is shown in Figure 1.

Table 2. Photo-initiated chemical vapor deposition (PICVD) process conditions to grow hydrophobic, hydrophilic, and vertical chemical gradient (VCG) coatings.

Wettability	Pressure (kPa)	Flow Rate (mL/min)	Gas Ratio (H_2/CO)	Time (min)	H_2O_2	Immediate Average Contact Angle
Hydrophobic	15	600	0.14	60	No	$125 \pm 3^\circ$
Hydrophilic	–15	600	0.14	60	Yes	$<5^\circ$
VCG	15/–15	600	0.14	180	No/Yes	$<5^\circ$

**Figure 1.** Schematic of the PICVD VCG (Photo-initiated chemical vapor deposition vertical chemical gradient) formed by a cross-linked hydrophobic layer beneath a hydrophilic coating.

2.2. Effect of Storage Conditions

The native contact angle of the SS-CNT was $125^\circ \pm 2$ (Table 2). Immediately following hydrophilic PICVD treatment, this value dropped to $<5^\circ$. This showed a complete transition from hydrophobic to superhydrophilic. As highlighted previously, one key mechanism for countering hydrophobic recovery relies on the stability of polar surface groups, which can be affected by storage conditions. Figure 2 highlights that the storage medium did not affect contact angle evolution in the first few days. However, after the tenth day, a clear separation was observed between both sample groups. Samples stored in water and air stabilized at contact angles of $50 \pm 4^\circ$ and $105 \pm 7^\circ$, respectively, after two months (Table 3). This suggested that long-term storage in a polar medium helped slow down hydrophobic recovery (by approximately half) but was not sufficient to maintain superhydrophilic behavior beyond one day. This can be explained by the fact that, over time, polymer chains containing polar functional groups can reorient and diffuse back towards the surface to be stabilized by dipole–dipole attraction

with polar water molecules surrounding the surface, effectively stabilizing the water contact angle [20]. This result was in accordance with that of Labonté et al., who observed an increased stability of PICVD-treated polystyrene beads upon storage in water [18]. Other works on PPFs have shown that polymer degradation is possible when stored in a polar medium. This can occur through the diffusion of water molecules into the film, leading to swelling or hydrolysis reactions with the polymer causing the dissolution of the film into the bulk of the medium [21]. This, however, was not observed in the case of PICVD films. If dissolution occurred, an increase in contact angle towards the initial CNT value should have been observed. In the case of air, hydrophobic functional groups are favored near the surface in order to reduce the surface energy [48]. Looking at the evolution of contact angle in Figure 2, and Figure 3, it can be seen that a sharp increase occurred during the first few days, eventually reaching a maximum. Afterwards, this value decreased and stabilized to a final value after two months. This behavior has been previously observed in plasma polymerized surfaces [17,49]. It can be explained as a competition between the restructuring and reorientation of surface chains and oxidation reactions with ambient air.

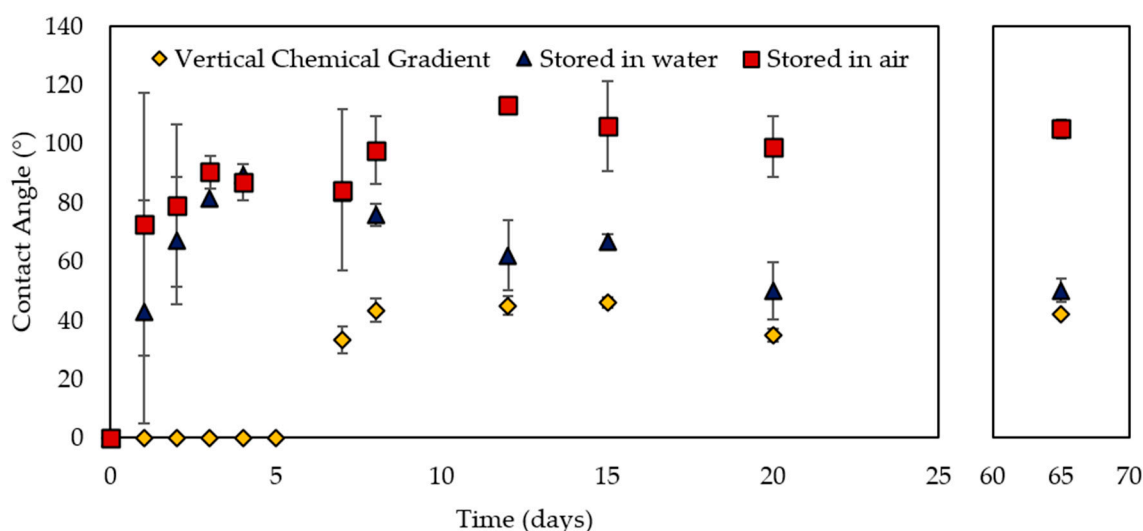


Figure 2. Contact angle aging of Photo-initiated chemical vapor deposition (PICVD) treatment on SS-CNT (carbon nanotube forest on stainless steel grids) samples.

Table 3. Water contact angle after 2 months. SS-CNT: carbon nanotube forest on stainless steel grids.

Sample	Contact Angle after 2 Months (°)
Bare SS-CNT	123 ± 3°
Air-stored hydrophilic SS-CNT	105 ± 7°
Water-stored hydrophilic SS-CNT	50 ± 4°
VCG SS-CNT	42 ± 1°

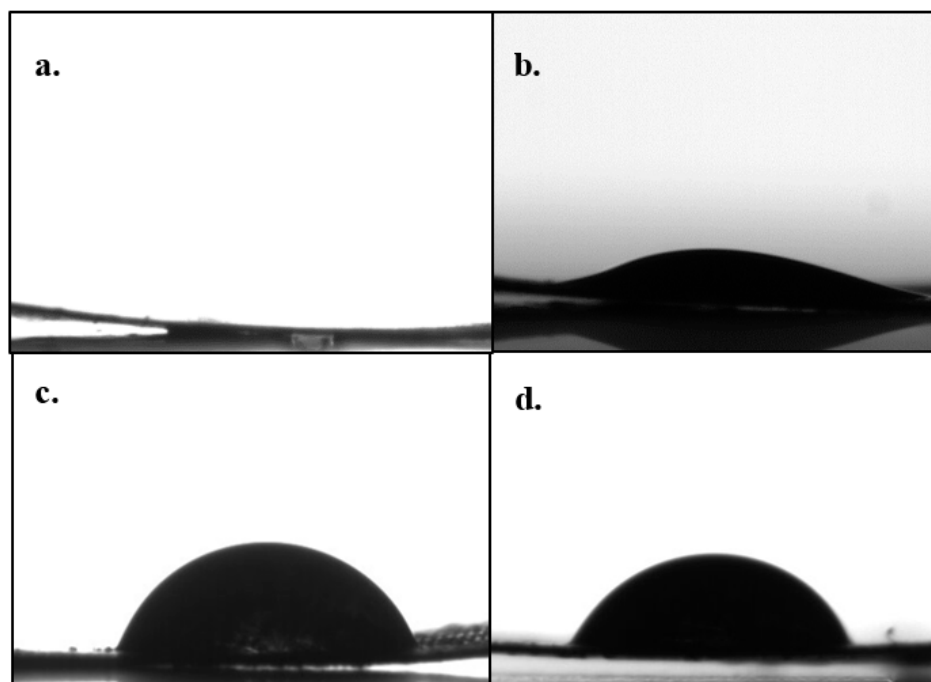


Figure 3. Water contact angle on SS-CNT (carbon nanotube forest on stainless steel grids) VCG (vertical chemical gradient)-treated samples, obtained through goniometry at (a) Day 0, (b) Day 6, (c) Day 15, and (d) 2 months after treatment.

In the first stage of contact angle evolution for the samples stored in both air and water, surface reorganization was the dominant mechanism [23,50,51]. Hydrophilic functional groups located at the surface tended to move towards the bulk, increasing the surface contact angle. This caused the contact angle to steeply increase in the first days post-functionalization. At the same time, an oxidation reaction with atmospheric oxygen introduced oxygen on the free radicals still present on the surface. This resulted in the incorporation of oxygenated groups at the surface that caused the contact angle to steadily decrease until full stabilization. This corresponded to the second stage, where, in the case of hydrophilic- and VCG-treated films, the contact angle slowly reduced towards a new equilibrium point. This stabilization process was also a function of the diffusivity of polymer chains in the film, which decreased with increasing cross-linking. Due to the slow deposition rate and the presence of UV light in PICVD, cross-linked structures were formed throughout treatment [50–52]. This may also have played a role in the slow diffusivity of polar groups, thus extending the time needed to stabilize at the surface. Finally, the stability of the contact angle measurements taken on the treated SS-CNT samples implied that the PICVD polymer films were not removed by surface interactions with water. This was also an indicator that the polymer structures had strong links with the SS-CNT substrate near the base of the film and the functional groups it contained near the surface. It has also been shown in previous work that PICVD coating bonds covalently with a variety of substrates. On silicon wafers, for example, Farhanian et al. evaluated Si–C bonds through the high resolution XPS of both carbon and silicon [47].

2.3. Effect of Surface Chemistry

By depositing a VCG film rather than a purely hydrophilic film, we observed that hydrophobic recovery was effectively suppressed for five days before wettability began to decrease (Figure 2). θ following VCG-PICVD stabilized to $42 \pm 1^\circ$ after two months of aging in air (Table 3). The stability of the film was likely due to the successful deposition of a highly cross-linked hydrophobic layer, enhanced by the longer deposition time and UV curing when compared to purely hydrophilic films. In VCG samples, this allows for the trapping of oxygenated functional groups at the surface and limiting their capability of reorienting or diffusing towards the bulk.

XPS was performed to correlate surface chemistry with the degree of hydrophobic recovery. Looking at the high resolution peak fittings of carbon C1s, four functionalities were observed at different binding energies: (1) 284.6 eV, associated with carbon sp^2 ; (2) 285.7 eV, corresponding to carbon sp^3 ; (3) 286.5 eV corresponding to carbon single-bonded to oxygen (C–O); and (4) 288 eV, which was indicative of carbon double-bonded to oxygen (C=O) and a π – π^* transition [52]. These binding energies were likely due to the incorporation of hydroxyl (–OH) and carboxyl (–COOH) groups representative of the oligomeric structure of the PICVD polymer film. Three functionalities were identified in the high-resolution O1s peaks: 529.8, 531.6, and 533.0 eV associated with metal oxide, O double-bonded to C, and O single-bonded to C, respectively (Figure 4c) [52]. In hydrophilic and VCG-treated samples, we observed distinct O–Fe and C=O peaks compared to hydrophobically-treated ones (Figure 4a). This, paired with the overall increase of O in the film, indicated a successful incorporation of oxygen-containing functional groups such as O–Fe, C–OH, –COOH, and C=O. This result was also valid for the VCG-treated SS-CNT samples. This result showed how the topmost layer of VCG films behaves hydrophilically for a longer duration of time than purely hydrophilic films.

The XPS analysis was reinforced by studying the near-surface oxygen-to-carbon ratio [O]/[C] (Figure 5): the [O]/[C] only decreased 30% over two months for the VCG sample, whereas it dropped by 51% and 86% for hydrophobic and hydrophilic samples, respectively. Upon the closer investigation of the Fe content in the films, we noticed similar behavior to that of O. Fe peaks appeared at 710.9 and 726 eV, corresponding to $Fe2p_{3/2}$ and $Fe2p_{1/2}$, respectively [52]. Furthermore, the couplings of the Fe peaks situated from 710.8–711 eV and O1s peaks at 529.8 were indicative of the formation of Fe oxides such as α - Fe_2O_3 or γ - Fe_2O_3 [53,54]. Similarly, Fe peaks at binding energy of 711.5 eV coupled with two distinct O peaks at 529.9 and 531.6 eV were associated with the formation of FeOOH [53,54]. Overall, Fe seemed to be present under its different oxidation states in the films.

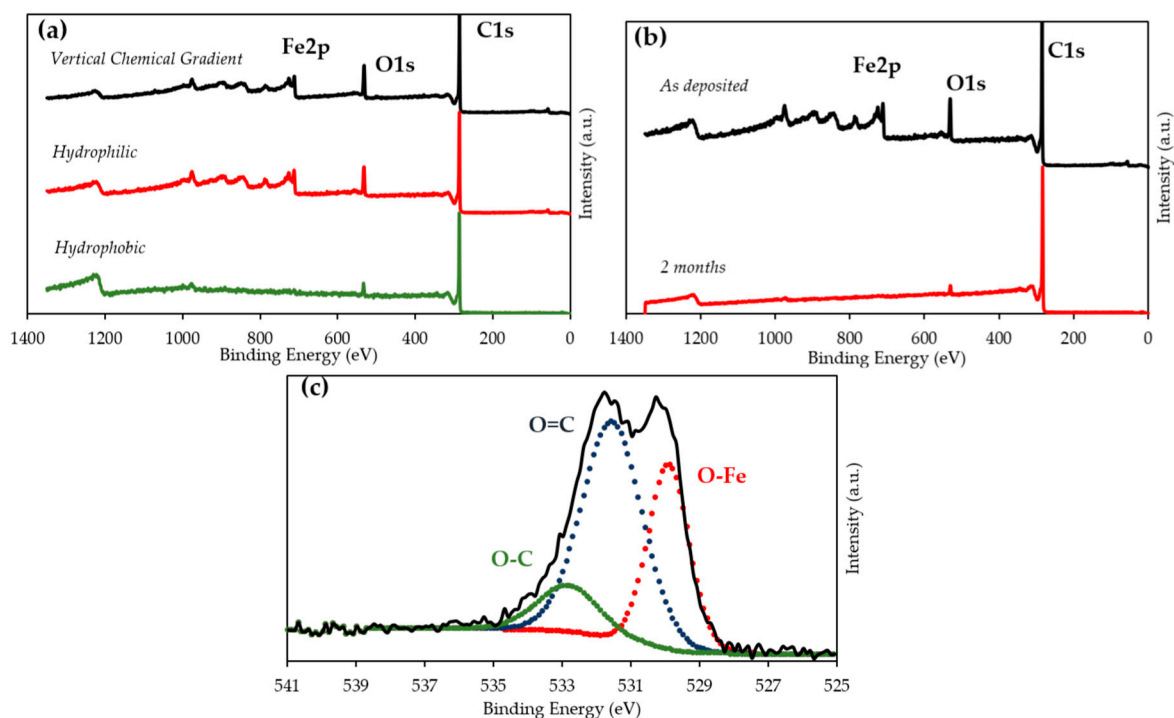


Figure 4. (a) XPS surveys for the Photo-initiated chemical vapor deposition PICVD-treated samples as deposited; (b) hydrophilic XPS survey as deposited and after 2 months; (c) high resolution O1s of the hydrophilic samples.

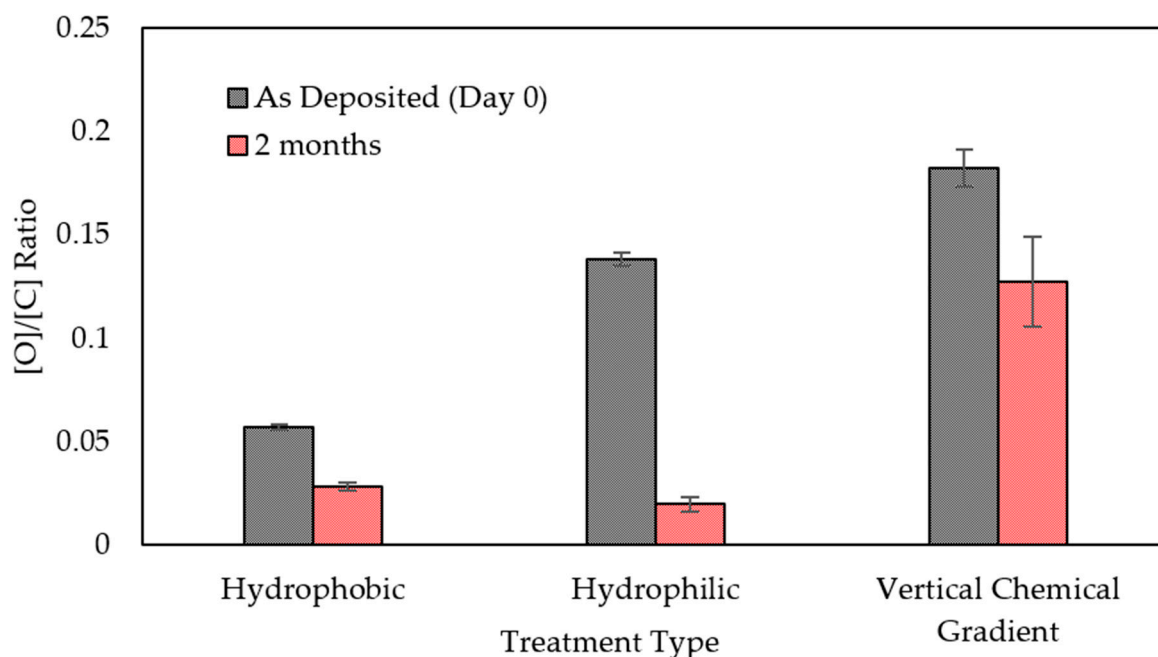


Figure 5. Aging of the coating observed thanks to the [O]/[C] ratio of PICVD (Photo-initiated chemical vapor deposition)-treated SS-CNTs (carbon nanotube forest on stainless steel grids) as deposited and after 2 months.

By analyzing Figure 4a and the elemental atomic percentages in Table 4, hydrophobic recovery can be observed in all samples, as indicated by the decrease of O over two months and the increase of C content at the surface. The difference lied in the starting amount of O in the films. As a reference, a hydrophobically PICVD-treated SS-CNT sample was prepared. By analyzing the XPS surveys for all three samples shown in Table 4, two major difference can be noticed: an increase in O content and appearance of Fe peaks between 700 and 740 eV. For all three substrates, O incorporation was associated with the formation of oxygenated functional groups, mainly from $\text{Fe}(\text{CO})_5$, H_2O_2 and partly from the CO precursor. The addition of H_2O_2 and the decrease in pressure therefore caused the observed increased O content in hydrophilic and VCG films. We observed a low relative atomic percentage of Fe on the surface because of the introduction of $\text{Fe}(\text{CO})_5$ in the PICVD reaction. Interestingly, these two observed features simultaneously disappeared after two months of storage (Figure 4b). These moieties seemed to play an important role in the degree of hydrophilicity of the final surface.

Table 4. Chemical composition of samples obtained through the XPS survey (full spectra provided as Supplementary Information in Figure S1, [Fe]/[C] ratio illustrated in Figure S2).

Sample	C1s			O1s			Fe2p		
	Day 0	Day 1	2 months	Day 0	Day 1	2 months	Day 0	Day 1	2 months
Hydrophobic	94.3%	-	97.2%	5.3%	-	2.71%	0.4%	-	0.11%
Hydrophilic	84.8%	-	97.6%	11.7%	-	2.38%	3.5%	-	0.07%
VCG	81.9%	79.6%	87.7%	14.9%	17.8%	11.13%	3.2%	2.6%	1.14%

In the hydrophobic reference case, very little O was incorporated into the polymer film, as expected, and a 49.3% decrease was measured after two months. For hydrophilic samples, this value was 79.7%, thus indicating the reversion from a hydrophilic, wettable surface back to a hydrophobic surface. In the case of the VCG samples, O contained near the surface of the film decreased by 25.4%, displaying an increased retention of O resulting in a higher stability in the hydrophilic PICVD treatment and a delayed or decelerated hydrophobic recovery.

3. Discussion

Oxygen was incorporated into the film through the various functional groups attached to the polymer chains. The decrease in the [O]/[C] ratio must then have been due to the reorganization of these chains at the air interface, since functional groups do not spontaneously detach from polymers. These oxygenated groups experience both short and long-range effects based on their immediate surroundings such as neighboring groups, the nature of the substrate, and the external media. Thus, their orientation is a crucial factor in the resulting wettability. When oxygenated moieties are facing away from the bulk, a surface will appear more hydrophilic [50]. Short-range motion, such as chain rotation around polymer backbone, is driven by both long-range attraction to other O contained within the bulk and repulsion from the air interface [50]. This alone, however, was not responsible for the decrease in O near the surface because storage in a polar medium would counter this short-range restructuring. Previous theoretical and simulation work has been done to gain a better understanding of polymer chain mobility in thin films. Generally, macromolecular mobility, namely diffusion, is enhanced near the surface [51]. There are several explanations for this, such as an enrichment of chain ends or lower chain packing density near the surface and the non-polar substrate [55,56]. In this study, this diffusion could be observed in all treatment types and storage mediums through the decrease in O. For samples stored in air, mobility would therefore have been enhanced at the air–film interface due to the repulsive nature between these two mediums. However, in the VCG samples, the [O]/[C] suffered less of a loss in O compared to the hydrophobic and, especially, hydrophilic ones. This was likely due to the fact that cross-linking in the base layer hindered the mobility of oxygenated groups and encouraged the hypothesis that a higher degree of cross-linking was achieved in the VCG samples. Cross-linking in polymer thin films can occur through several mechanisms depending on compounds and functional groups contained within the film. One way cross-linking occurs is through hydrogen bonding, which can occur between hydroxyl and carboxyls inside PICVD thin films [56]. Metal coordination can also occur between Fe ions incorporated by a $\text{Fe}(\text{CO})_5$ precursor and polar functional groups in a polymer structure. It was found that these metal–ligand interactions were stable at room temperature. However, these noncovalent interactions disappeared at slightly higher temperatures (30 °C). This also hinted at the increased mobility of Fe. In PICVD, cross-linking via UV irradiation (photo cross-linking) also occurs. As polymer chains are formed in a film, they may grow through addition with a neighboring chain [57]. However, in radical polymerization, the high density of reactive radicals formed under UV favor intermolecular and intramolecular reactions. These lead to a highly cross-linked product. In this case, the dimerization of carboxyl groups may have occurred, thus resulting in the attachment of two individual polymer chains [58]. Additionally, through these processes, radical trapping in restrained spaces in cross-linked structures may occur due to steric hinderance [57]. These may be radicals that are bonded to the bulk structure or alone. This adds to the fact that post treatment mobility can occur through the radical conversion of these loosely bonded groups. In this case, oxygen found near the surface layer was reduced. Another parameter that influences photo cross-linking is irradiation time. Previous studies on photo cross-linking have shown that increased irradiation time significantly reduces O permeability [58,59]. As cross-linking increases within the polymer structure, the rotational movement of functional groups around the C–C backbone is significantly reduced due to the additional bonding that effectively restricts this type of movement [50]. Diffusion within the PICVD film also depends on the free volume within the film [60]. Increased open space within the polymer matrix therefore leads to a higher amount of O diffusion. It is well known that cross-linking within the polymer structure reduces the free volume and, as a result, limits the segmental mobility.

Despite the current inability to maintain the superhydrophilic quality of VCG samples, employing the bilayer strategy can increase the hydrophilic stability window for five days. Similar works have shown stabilization in hydrophilic regions. It is, however, difficult to compare the results obtained in this study with other work due to the variability in surfaces and methodology. In our work, starting with carbonaceous material that was intrinsically hydrophobic, we showed a drastic change in wettability (~100% decrease from native value). In PICVD deposited films, superhydrophilicity is

achieved through the incorporation of a high number of oxygenated groups that adsorb and grow on the substrate. This is also enhanced by the high surface area of the CNT forest. This allows for a higher amount of available hydrophilic sites onto which water can spread once the deposition is made. From this modified state, hydrophobic recovery does not appear until five days later. Such results were demonstrated with PDMS thin films by Vlachopoulou et al. [61]. In an inductively coupled plasma reactor, they were able to create completely wetted surfaces by first generating nanostructures through etching with sulfide hexafluoride (SF_6) plasma followed by a functionalization step in O_2 plasma. This technique produced completely wetted surfaces ($<5^\circ$) that lasted for seven days. They found that nanostructuring the surface was an important factor in suppressing hydrophobic recovery [61]. This led us to believe that a similar phenomenon occurs with SS-CNT surfaces that are intrinsically nanostructured. The degree of hydrophobic recovery can be expressed as the total increase of contact angle from an initially functionalized surface relative to the angle at which it stabilizes once the effect of recovery is no longer observed. When looking at the degree of hydrophobic recovery, VCG samples start from $<5^\circ$ and stabilize at $\sim 42^\circ$ after 1440 h (2 months). From this perspective, it seems as though hydrophobic recovery is still a dominating phenomenon upon its onset. This value, however, also depends on the starting contact angle of a surface post-functionalization. In the work of Rupper et al., for instance, hydrophilic Si wafers with contact angles that aged from approximately 41 to 45° after 5000 h (7 months) were produced by applying VCG PPFs [33]. Though the degree of hydrophobic recovery was only of 9.8%, the hydrophilicity achieved after treatment was lower when compared to the results presented in this study. The surface modification was more pronounced in the case of SS-CNT substrates, going from approximately 120° to $<5^\circ$, corresponding to almost 100% reduction in contact angle, whereas the native contact angle of argon cleaned Si wafers ($\sim 70^\circ$) was reduced by 41.4%. Past preliminary observations on hydrophobic recovery of PICVD hydrophilic films on high density polyethylene (HDPE) extrusion nets showed that full hydrophobic recovery is always achieved for samples stored in air [47]. Seeing as this is also the case for SS-CNT substrates, this shows that the nature of the substrate is not sufficient to minimize the degree of hydrophobic recovery and that the chemical nature of the polymeric film itself is dominant. This has been further shown with VCG samples, where the chemistry differs in the deposition and storage in air leads to improved stability. Previous PICVD studies have used polystyrene (PS) beads [18]. Interestingly, hydrophilicity has been shown to be maintained for a longer duration using SS-CNT substrates when compared to hydrophilically-treated PS beads that were also stored in water. This further showed how the nanostructuring of a surface may help reduce the degree of hydrophobic recovery on a surface.

$\text{Fe}(\text{CO})_5$ also appeared to play a significant role in the behavior of the PICVD generated films. This compound was formed from the reaction of CO with the steel walls of the CO gas cylinder. It is known that Fe and Ni carbonyls can form over extended periods of time at low temperatures and high pressures [44,62–64]. For a photochemical reaction to occur, a compound must satisfy two conditions. First, there must be an overlap between the spectral emission of the light source and the absorption spectrum of the targeted molecule. Second, the absorbed photon must have enough energy to initiate the reaction. Incidentally, $\text{Fe}(\text{CO})_5$ absorbs light in the UV spectrum and has a bond dissociation energy of 55 kcal/mol corresponding to 519.84 nm (in other words, light with shorter wavelengths has sufficient energy for bond scission) [29,65]. Therefore under the 253.7 and 185 nm light emitted by low pressure Hg UVC lamps, it loses its CO groups through photofragmentation to form reactive intermediates such as $\text{Fe}(\text{CO})_4$, $\text{Fe}(\text{CO})_3$, and $\text{Fe}(\text{CO})_2$. These intermediates react in the gas phase with other species such as -OH radicals that are generated through the photodissociation of H_2O_2 forming a wide variety of compounds. These finally adsorb onto the substrate and react with C and O groups, as well as other surrounding Fe compounds to form secondary and tertiary oxides [44,47]. A previous analysis of this compound in our experimental setup found that it was present in the reaction mixture between 0.02 and 6.7 ppm [44]. Despite these low quantities, it was clear from the results obtained that the $\text{Fe}(\text{CO})_5$ acted as a homogeneous photocatalyst that was crucial for the development of stable PICVD coatings, especially in the hydrophilic case. The lack of controllability of this compound

stood out as an important aspect to improve upon in the future. Its catalytic properties have been extensively studied in the past. Water gas shift, olefin isomerization, direct liquefaction, and alkene hydrogenation reactions are some examples of the use of $\text{Fe}(\text{CO})_5$ as a catalyst [66–68]. In the case of water gas shift reactions, for instance, reaction rates have a proportional relationship with $\text{Fe}(\text{CO})_5$ concentration [69,70]. Additionally, a reduction in activation energies was also reported. In this work, an increase in $\text{Fe}(\text{CO})_5$ concentration resulted in a higher formation of iron carbonyl radicals and increased the reaction rates for -OH generation. Upon photodissociation, secondary and tertiary iron compounds can catalyze photo-Fenton reactions with H_2O_2 [71]. Thus, hydroxyl radical generation is accelerated through the addition of $\text{Fe}(\text{CO})_5$. This is particularly interesting considering that, in this case, Fe content in the hydrophobic PICVD films was lower than in hydrophilic PICVD films. Seeing as no H_2O_2 was present in hydrophobic treatments, Fe carbonyls present in the reaction mixture exhibited less catalytic behavior.

Furthermore, Fe atoms that were incorporated into the polymer film also appeared to leave the surface after two months, as shown in the XPS spectrum. Basic diffusion could have resulted from concentration gradients, and, in this case, it would be possible that Fe diffused back into the bulk of the film to achieve a lower energy state equilibrium [72]. This was possible considering the low amount of Fe found in hydrophobic coatings, generating a gradient between the top layer of the film and the bulk. As a hydrophilic film transitions from hydrophilic to hydrophobic, Fe can thus dig its way as a result of the diffusion and reorientation mechanisms commonly responsible for hydrophobic recovery. Transition metal diffusion into polymers has been investigated by many research groups, typically in the field of microelectronics [73,74]. However, there is uncertainty whether metals truly diffuse into polymers or rather agglomerate [73]. Briefly, metal–metal cohesive energy is generally two orders of magnitude higher than that of polymers. This favors metal–metal interactions rather than metal–polymer mixing [73]. Thus, agglomerates are expected to be formed at equilibrium conditions. Faupel et al. studied the interaction of Cu in polyimide films through XPS and noticed a decrease in Cu intensity after annealing [74]. In this case, diffusion was ruled out in favor of Cu clustering, and the decrease of intensity was attributed to inelastic scattering of photoelectrons in the newly formed agglomerates [74]. This exemplifies the difficulty in appropriately assessing metal–polymer interactions. In our case, however, we observed, for hydrophilic coatings, that Fe peaks could no longer be seen after two months. It therefore seemed that diffusion was the major mechanism at play since the decrease in Fe was quasi-total. This can be explained through Gibbs free energy. Generally, a higher cohesive energy results in a high surface energy [73–75]. For metal particles, Gibbs free energy is lower when it is surrounded by other metals or polymer molecules compared to when it is situated at the air interface (i.e., as deposited). Thus, it is possible that Fe atoms diffuse below the top layer into the bulk when the surface tension of the metal is higher than the sum of both the polymer surface tension and the metal–polymer interfacial tension [73]. As mentioned previously, polymer cohesive energy is considerably lower than metal cohesive energy, resulting in lower polymer surface tension. Therefore, both Fe and polymer compounds look to interact with other Fe compounds first, then with polymer, and then with air. However, it is possible that Fe atoms are still pulled inwards due to long range Van der Waals force stemming from the fact that there is more polymer in the bulk than near the surface [73]. The loss of Fe in this process may therefore come from a combination of both diffusion towards the bulk of the film and, possibly, agglomeration, thus effectively lowering the intensity observed through XPS.

4. Materials and Methods

4.1. Carbon Nanotube (CNT) Growth

Type 316 stainless steel (SS) meshes (400 mesh size) were purchased from McMaster-Carr. The direct growth of CNT on the stainless steel meshes was done by thermal chemical vapor deposition following methodology developed from the past work of Baddour et al. and Horody et al. [76,77]. The SS grids were cut into 2.5 by 8 cm strips and ultrasonically cleaned in an acetone bath for 10 min.

These were then inserted into preheated 700 °C furnace. The furnace was first purged with Argon (Ar, 99.9%, MEGS, Montreal, QC, Canada) for 5 min at a rate of 3.14 L/min to remove any present oxygen. Subsequently, Ar flow was reduced to 0.592 L/min, and acetylene (C_2H_2 , MEGS, Montreal, QC, Canada) was introduced at a flow rate of 0.068 L/min for 2 min. C_2H_2 flow was stopped, and the furnace allowed to stagnate for 2 min (corresponds to the CNT growth phase). The reactor was then purged with Ar at 3.14 L/min for 5 min, and the stainless steel grids covered with CNT (SS-CNT) were removed from the furnace [77].

4.2. Photo-Initiated Chemical Vapor Deposition (PICVD)

The custom-made PICVD reactor consisted of a quartz tube with a length of 50 cm and a 25 mm diameter illuminated by two UVC, low-pressure, germicidal lamps (Figure 6). These lamps' primary emission peak was at 253.7 nm with a weaker, secondary peak at 185 nm. Total irradiance was 0.01 W/cm² at 3.5 cm. The photo-initiator, H_2O_2 (50% w/w, Fisher Scientific, Montreal, QC, Canada), was injected into the reactor using a syringe pump (New Era Instruments, Farmingdale, NY, USA) at a rate of 1 μ L/hour in the case of the hydrophilic treatments (or second phase of the VCG). Mass flow controllers (Brooks by Polycontrols, Brossard, QC, Canada) regulated the precursor gas flow, namely syngas, composed of hydrogen (H_2 , 99.97%, Air Liquide, Montreal, QC, Canada) and carbon monoxide (CO , 99.97%, Air Liquide, Montreal, QC, Canada), and the purging gas (Ar, 99.9%, Air Liquide, Montreal, QC, Canada). Before all experiments (see parameters retained in Table 4), the reactor was purged with Ar for 3 min at 3 L/min. Processing was undertaken at room temperature (23 °C). An increase in temperature up to ~50 °C was recorded due to the heat given off by the UVC lamps to the reactor over the 60–180 min treatments. Each experiment was repeated three times to ensure the reproducibility and to calculate the uncertainty of measurements.

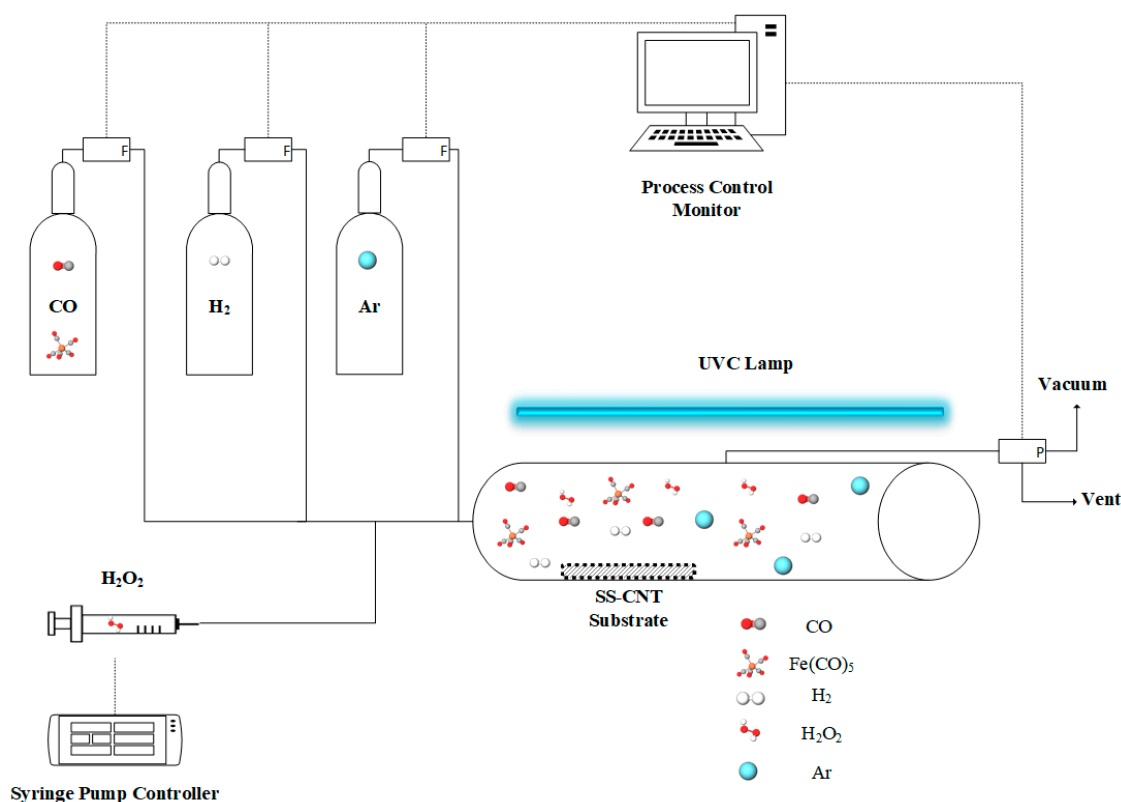


Figure 6. Photo-initiated chemical vapor deposition (PICVD) experimental setup.

4.3. Surface Characterization

The surface contact angle (θ) and surface energy were measured with an FDS OCA-20 tensiometer (Dataphysics, Filderstadt, Germany). For this, water droplets of 1 μL , grown at a rate of 0.1 $\mu\text{L/s}$, were directly deposited on level samples. This was performed at 3 different regions and repeated 3 times to calculate the average θ .

X-ray photoelectron spectroscopy was done using a Thermo Scientific K-Alpha system with an aluminum X-ray source on a 400 μm size area. A first survey scan was done on each sample to determine the elements that were present. This was then followed by a high resolution (HR) pass in order to obtain detailed spectra for both carbon (C 1s) and oxygen (O 1s).

5. Conclusions

This work has shown that hydrophobic recovery can be delayed from zero to five days post-PICVD functionalization by using a vertical chemical gradient within a polymer film. It was assumed that this gradient started as a hydrophobic, heavily cross-linked structure near the substrate and slowly shifted towards a less cross-linked oxygenated layer near the environment-exposed surface. This was proven on SS-CNT substrates, which were chosen for their high specific surface area that could eventually be beneficial in a wide range of applications. It would be important to push this work to achieve full stability over an extended to unlimited period. To do this, it would be necessary to study the nature of the PICVD film, especially its cross-linking density through swelling tests. From there, it would be pertinent to look more closely at the cross-linking within the polymeric deposition by employing common photo-crosslinkers such as benzophenone in the photo-initiated process or by studying the kinetics of photo-curing during and post-illumination, which can give crucial insight into the cross-linking density. We also observed Fe incorporation in the thin film, originating from Fe pentacarbonyl formation in the CO gas cylinder, that is known to be photo-active under UVC irradiation and thus plays an important role in the process. The control of the insertion of this compound in the system is important to study in future work. This work has presented a first step to studying the repression of hydrophobic recovery in PICVD-treated surfaces. The degree to which this phenomenon should be suppressed will likely depend on the intended application. Taking anti-fouling as an example, increased free surface energy is required to limit the growth of microorganisms on surfaces. In the case of ships submerged in water, hydrophilic and VCG samples show potential in maintaining a good degree of hydrophilicity. This is especially true because hydrophilic states are more stable in polar solutions such as water.

Supplementary Materials: The following are available online at <http://www.mdpi.com/2073-4344/10/5/534/s1>, Figure S1: XPS - C1s and O1s peaks; Figure S2: [Fe]/[C] Ratio.

Author Contributions: Conceptualization, J.R.T. and A.A.; methodology, J.R.T. and A.A.; investigation, A.A.; resources, J.R.T. and U.L.; writing—original draft preparation, A.A.; writing—review and editing, A.A., U.L., J.-L.M. and J.R.T.; supervision, J.-L.M. and J.R.T.; project administration, J.R.T.; All authors have read and agreed to the published version of the manuscript.

Funding: This research was funded by NSERC (grant CRD-522391), Prima (grant R16-46-003) and Awn Nanotech.

Acknowledgments: We wish to acknowledge the financial support provided by the Natural Sciences and Engineering Research Council (NSERC), Prima and Awn Nanotech. We would also like also to thank McGill University (Plasma Processing Laboratory) for allowing us to use their furnace. The authors acknowledge the collaboration of Wendell Raphael (Polytechnique Montreal) for his assistance and expertise in PICVD experiments.

Conflicts of Interest: The authors declare no conflict of interest.

References

1. Zhang, S.; Huang, J.; Chen, Z.; Lai, Y. Bioinspired Special Wettability Surfaces: From Fundamental Research to Water Harvesting Applications. *Small* **2017**, *13*, 1–28. [CrossRef]
2. Drelich, J.; Chibowski, E.; Meng, D.D.; Terpilowski, K. Hydrophilic and superhydrophilic surfaces and materials. *Soft Matter* **2011**, *7*, 9804–9828. [CrossRef]

3. Ueda, E.; Levkin, P.A. Emerging applications of superhydrophilic-superhydrophobic micropatterns. *Adv. Mater.* **2013**, *25*, 1234–1247. [[CrossRef](#)] [[PubMed](#)]
4. Si, Y.; Dong, Z.; Jiang, L. Bioinspired Designs of Superhydrophobic and Superhydrophilic Materials. *ACS Cent. Sci.* **2018**, *4*, 1102–1112. [[CrossRef](#)] [[PubMed](#)]
5. Otitoju, T.A.; Ahmad, A.L.; Ooi, B.S. Superhydrophilic (superwetting) surfaces: A review on fabrication and application. *J. Ind. Eng. Chem.* **2017**, *47*, 19–40. [[CrossRef](#)]
6. Yu, Z.; Yun, F.F.; Wang, Y.; Yao, L.; Dou, S.; Liu, K.; Jiang, L.; Wang, X. Desert Beetle-Inspired Superwetable Patterned Surfaces for Water Harvesting. *Small* **2017**, *13*, 1–6. [[CrossRef](#)]
7. Salta, M.; Wharton, J.A.; Stoodley, P.; Dennington, S.P.; Goodes, L.R.; Werwinski, S.; Mart, U.; Wood, R.J.K.; Stokes, K.R. Designing biomimetic antifouling surfaces. *Philos. Trans. R. Soc. A Math. Phys. Eng. Sci.* **2010**, *368*, 4729–4754. [[CrossRef](#)]
8. Nurioglu, A.G.; Esteves, A.C.C.; De With, G. Non-toxic, non-biocide-release antifouling coatings based on molecular structure design for marine applications. *J. Mater. Chem. B* **2015**, *3*, 6547–6570. [[CrossRef](#)] [[PubMed](#)]
9. Thomas, K.V.; Brooks, S. The environmental fate and effects of antifouling paint biocides. *Biofouling* **2010**, *26*, 73–88. [[CrossRef](#)]
10. Chiavarini, S.; Ubaldi, C.; Cannarsa, S. Biocides in antifouling paints: Environmental concentration levels and distribution. *Energia Ambiente e Innovazione* **2014**, 52–56. [[CrossRef](#)]
11. Majhy, B.; Iqbal, R.; Sen, A.K. Facile fabrication and mechanistic understanding of a transparent reversible superhydrophobic – superhydrophilic surface. *Sci. Rep.* **2018**, *8*, 1–11. [[CrossRef](#)] [[PubMed](#)]
12. Zhang, L.; Zhao, N.; Xu, J. Fabrication and application of superhydrophilic surfaces: A review. *J. Adhes. Sci. Technol.* **2014**, *28*, 769–790. [[CrossRef](#)]
13. Andrade, J.D.; Smith, L.M.; Gregonis, D.E. The Contact Angle and Interface Energetics. In *Surface and Interfacial Aspects of Biomedical Polymers*; Plenum Press: New York, NY, USA, 1985; pp. 249–292.
14. Everaert, E.P.; Van Der Mei, H.C.; Busscher, H.J. Hydrophobic recovery of repeatedly plasma-treated silicone rubber. Part 2. A comparison of the hydrophobic recovery in air, water, or liquid nitrogen. *J. Adhes. Sci. Technol.* **1996**, *10*, 351–359. [[CrossRef](#)]
15. Granick, S. Polymer surface dynamics. *MRS Bull.* **1996**, *21*, 33–36. [[CrossRef](#)]
16. Morra, M.; Occhiello, E.; Garbassi, F. Contact Angle Hysteresis in Oxygen Plasma Treated Poly(tetrafluoroethylene). *Langmuir* **1989**, *5*, 872–876. [[CrossRef](#)]
17. Van Os, M.T. *Surface Modification by Plasma Polymerization: Film Deposition, Tailoring of Surface Properties and Biocompatibility*; Universiteit Twente: Enschede, The Netherlands, 2000.
18. Labonté, V.; Marion, A.; Virgilio, N.; Tavares, J.R. Gas-phase surface engineering of polystyrene beads used to challenge automated particle inspection systems. *Ind. Eng. Chem. Res.* **2016**, *55*, 7362–7372. [[CrossRef](#)]
19. Borgia, C.; Punga, I.L.; Borgia, G. Surface properties and hydrophobic recovery of polymers treated by atmospheric-pressure plasma. *Appl. Surf. Sci.* **2014**, *317*, 103–110. [[CrossRef](#)]
20. Bormashenko, E.; Chaniel, G.; Grynyov, R. Towards understanding hydrophobic recovery of plasma treated polymers: Storing in high polarity liquids suppresses hydrophobic recovery. *Appl. Surf. Sci.* **2013**, *273*, 549–553. [[CrossRef](#)]
21. Vandenbossche, M.; Hegemann, D. Recent approaches to reduce aging phenomena in oxygen- and nitrogen-containing plasma polymer films: An overview. *Curr. Opin. Solid State Mater. Sci.* **2018**, *22*, 26–38. [[CrossRef](#)]
22. Hegemann, D.; Michlíček, M.; Blanchard, N.E.; Schütz, U.; Lohmann, D.; Vandenbossche, M.; Zajíčková, L.; Drábik, M. Deposition of Functional Plasma Polymers Influenced by Reactor Geometry in Capacitively Coupled Discharges. *Plasma Process. Polym.* **2016**, *13*, 279–286. [[CrossRef](#)]
23. Hegemann, D.; Lorusso, E.; Butron-Garcia, M.I.; Blanchard, N.E.; Rupper, P.; Favia, P.; Heuberger, M.; Vandenbossche, M. Suppression of Hydrophobic Recovery by Plasma Polymer Films with Vertical Chemical Gradients. *Langmuir* **2016**, *32*, 651–654. [[CrossRef](#)] [[PubMed](#)]
24. Holly, F.J.; Refojo, M.F. Wettability of hydrogels I. Poly(2-hydroxyethyl methacrylate). *J. Biomed. Mater. Res.* **1975**, *9*, 315–326. [[CrossRef](#)] [[PubMed](#)]
25. Deng, L.; Li, Y.; Feng, F.; Zhang, H. Study on wettability, mechanical property and biocompatibility of electrospun gelatin/zein nanofibers cross-linked by glucose. *Food Hydrocoll.* **2019**, *87*, 1–10. [[CrossRef](#)]

26. Spruell, J.M.; Wolffs, M.; Leibfarth, F.A.; Stahl, B.C.; Heo, J.; Connal, L.A.; Hu, J.; Hawker, C.J. Reactive, multifunctional polymer films through thermal cross-linking of orthogonal click groups. *J. Am. Chem. Soc.* **2011**, *133*, 16698–16706. [[CrossRef](#)] [[PubMed](#)]
27. Owen, M.J.; Smith, P.J. Plasma treatment of polydimethylsiloxane. *J. Adhes. Sci. Technol.* **1994**, *8*, 1063–1075. [[CrossRef](#)]
28. Everaert, E.P.; van der Mei, H.C.; De Vries, J.; Busscher, H.J. Hydrophobic recovery of repeatedly plasma-treated silicone rubber. Part 1. Storage in air. *J. Adhes. Sci. Technol.* **1995**, *9*, 1263–1278. [[CrossRef](#)]
29. Marquez, A.; Daniel, C.; Sanz, J.F. The vacuum-ultraviolet spectrum of Fe(CO)₅: An experimental analysis supported by a CASSCF CCI study of the Rydberg states. *J. Phys. Chem.* **1992**, *96*, 121–123. [[CrossRef](#)]
30. Zhang, Y.; Kobayashi, I.; Neves, M.A.; Uemura, K.; Nakajima, M. Effects of surface treatment and storage conditions of silicon microchannel emulsification plates on their surface hydrophilicity and preparation of soybean oil-in-water emulsion droplets. *J. Food Eng.* **2015**, *167*, 106–113. [[CrossRef](#)]
31. Lavielle, L.; Schultz, J. Surface properties of graft polyethylene in contact with water. I. Orientation phenomena. *J. Colloid Interface Sci.* **1985**, *106*, 438–445. [[CrossRef](#)]
32. Vergelati, C.; Perwuelz, A.; Vovelle, L.; Romero, M.A.; Holl, Y. Poly(ethylene terephthalate) surface dynamics in air and water studied by tensiometry and molecular modelling. *Polymer (Guildf)*. **1994**, *35*, 262–270. [[CrossRef](#)]
33. Rupper, P.; Vandenbossche, M.; Bernard, L.; Hegemann, D.; Heuberger, M. Composition and Stability of Plasma Polymer Films Exhibiting Vertical Chemical Gradients. *Langmuir* **2017**, *33*, 2340–2352. [[CrossRef](#)] [[PubMed](#)]
34. Li, L.; Dai, X.J.; Xu, H.S.; Zhao, J.H.; Yang, P.; Maurdev, G.; Du Plessis, J.; Lamb, P.R.; Fox, B.L.; Michalski, W.P. Combined continuous wave and pulsed plasma modes: For more stable interfaces with higher functionality on metal and semiconductor surfaces. *Plasma Process. Polym.* **2009**, *6*, 615–619. [[CrossRef](#)]
35. Yousif, E.; Haddad, R. Photodegradation and photostabilization of polymers, especially polystyrene: Review. *Springerplus* **2013**, *2*, 1–32. [[CrossRef](#)] [[PubMed](#)]
36. Hedenqvist, M.S. Barrier packaging materials. In *Handbook of Environmental Degradation of Materials*; William Andrew Publishing: Norwich, NY, USA, 2005; pp. 547–563.
37. Galant, O.; Davidovich-Pinhas, M.; Diesendruck, C.E. The Effect of Intramolecular Cross-Linking on Polymer Interactions in Solution. *Macromol. Rapid Commun.* **2018**, *39*, 1–5. [[CrossRef](#)] [[PubMed](#)]
38. Dorval Dion, C.A.; Raphael, W.; Tong, E.; Tavares, J.R. Photo-initiated chemical vapor deposition of thin films using syngas for the functionalization of surfaces at room temperature and near-atmospheric pressure. *Surf. Coatings Technol.* **2014**, *244*, 98–108. [[CrossRef](#)]
39. Chan, K.; Gleason, K.K. Photoinitiated chemical vapor deposition of polymeric thin films using a volatile photoinitiator. *Langmuir* **2005**, *21*, 11773–11779. [[CrossRef](#)]
40. McMahon, B.J.; Pfluger, C.A.; Sun, B.; Ziemer, K.S.; Burkey, D.D.; Carrier, R.L. Photoinitiated chemical vapor deposition of cytocompatible poly(2-hydroxyethyl methacrylate) films. *J. Biomed. Mater. Res. - Part A* **2014**, *102*, 2375–2382. [[CrossRef](#)]
41. Baxamusa, S.H. Photoinitiated Chemical Vapor Deposition [sic]: Mechanism and Applications. Ph.D. Thesis, Massachusetts Institute of Technology, Cambridge, MA, USA, 2009.
42. Zhao, J.; Wang, M.; Gleason, K.K. Stabilizing the Wettability of Initiated Chemical Vapor Deposited (iCVD) Polydivinylbenzene Thin Films by Thermal Annealing. *Adv. Mater. Interfaces* **2017**, *4*, 1–9. [[CrossRef](#)]
43. Lari, H.N.; Chaouki, J.; Tavares, J.R. Continuous aerosol photopolymerization to coat de-agglomerated nanoparticles. *Chem. Eng. J.* **2020**, *390*, 124526. [[CrossRef](#)]
44. Nasri Lari, H.; Farhanian, D.; Boffito, D.C.; Patience, G.S.; De Crescenzo, G.; Chaouki, J.; Tavares, J.R. Shedding light on iron pentacarbonyl photochemistry through a CVD case study. *Catal. Commun.* **2017**, *100*, 19–23. [[CrossRef](#)]
45. Hosseininasab, S.; Faucheux, N.; Soucy, G.; Tavares, J.R. Full range of wettability through surface modification of single-wall carbon nanotubes by photo-initiated chemical vapour deposition. *Chem. Eng. J.* **2017**, *325*, 101–113. [[CrossRef](#)]
46. Berard, A.; Patience, G.S.; Chouinard, G.; Tavares, J.R. Photo Initiated Chemical Vapour Deposition to Increase Polymer Hydrophobicity. *Sci. Rep.* **2016**, *6*, 1–9. [[CrossRef](#)] [[PubMed](#)]
47. Farhanian, D.; De Crescenzo, G.; Tavares, J.R. Kinetics, Chemistry, and Morphology of Syngas Photoinitiated Chemical Vapor Deposition. *Langmuir* **2017**, *33*, 1780–1791. [[CrossRef](#)] [[PubMed](#)]

48. Petruczuk, C.D.; Armagan, E.; Ince, G.O.; Gleason, K.K. Initiated chemical vapor deposition and light-responsive cross-linking of poly(vinyl cinnamate) thin films. *Macromol. Rapid Commun.* **2014**, *35*, 1345–1350. [[CrossRef](#)]
49. Senzai, T.; Fujikawa, S. Fast hydrophobicity recovery of the surface-hydrophilic poly(dimethylsiloxane) films caused by rechemisorption of dimethylsiloxane derivatives. *Langmuir* **2019**, *35*, 9747–9752. [[CrossRef](#)]
50. Yasuda, H.; Sharma, A.K.; Yasuda, T. Effect of Orientation and Mobility of Polymer Molecules At Surfaces on Contact Angle and Its Hysteresis. *J. Polym. Sci. Part A-2 Polym. Phys.* **1981**, *19*, 1285–1291. [[CrossRef](#)]
51. Tseng, K.C.; Turro, N.J.; Durning, C.J. Molecular mobility in polymer thin films. *Phys. Rev. E Stat. Phys. Plasmas Fluids Relat. Interdiscip. Top.* **2000**, *61*, 1800–1811. [[CrossRef](#)]
52. Briggs, D. *Handbook of X-ray Photoelectron Spectroscopy*; Wanger, C.D., Riggs, W.M., Davis, L.E., Moulder, J.F., Muilenberg, G.E., Eds.; Perkin-Elmer Corp., Physical Electronics Division: Eden Prairie, MN, USA, 1979; pp. 190–195.
53. Grosvenor, A.P.; Kobe, B.A.; Biesinger, M.C.; McIntyre, N.S. Investigation of multiplet splitting of Fe 2p XPS spectra and bonding in iron compounds. *Surf. Interface Anal.* **2004**, *36*, 1564–1574. [[CrossRef](#)]
54. Oswald, S. X-Ray Photoelectron Spectroscopy in Analysis of Surfaces. In *Encyclopedia of Analytical Chemistry: Applications, Theory, and Instrumentation*; John Wiley & Sons, Ltd.: Hoboken, NJ, USA, 2013; ISBN 9780470027318.
55. Kerle, T.; Lin, Z.; Kim, H.C.; Russell, T.P. Mobility of polymers at the air/polymer interface. *Macromolecules* **2001**, *34*, 3484–3492. [[CrossRef](#)]
56. Hu, W.; Wang, Z.; Xiao, Y.; Zhang, S.; Wang, J. Advances in crosslinking strategies of biomedical hydrogels. *Biomater. Sci.* **2019**, *7*, 843–855. [[CrossRef](#)]
57. Andrzejewska, E. Photopolymerization kinetics of multifunctional monomers. *Prog. Polym. Sci.* **2001**, *26*, 605–665. [[CrossRef](#)]
58. Hunger, K.; Schmeling, N.; Jeazet, H.B.T.; Janiak, C.; Staudt, C.; Kleinermanns, K. Investigation of cross-linked and additive containing polymer materials for membranes with improved performance in pervaporation and gas separation. *Membranes (Basel)*. **2012**, *2*, 727–763. [[CrossRef](#)] [[PubMed](#)]
59. Kang, J.S.; Won, J.; Park, H.C.; Kim, U.Y.; Kang, Y.S.; Lee, Y.M. Morphology control of asymmetric membranes by UV irradiation on polyimide dope solution. *J. Memb. Sci.* **2000**, *169*, 229–235. [[CrossRef](#)]
60. Boersma, A.; Cangialosi, D.; Picken, S.J. Mobility and solubility of antioxidants and oxygen in glassy polymers II. Influence of physical ageing on antioxidant and oxygen mobility. *Polym. Degrad. Stab.* **2003**, *79*, 427–438. [[CrossRef](#)]
61. Vlachopoulou, M.E.; Petrou, P.S.; Kakabakos, S.E.; Tserepi, A.; Beltsios, K.; Gogolides, E. Effect of surface nanostructuring of PDMS on wetting properties, hydrophobic recovery and protein adsorption. *Microelectron. Eng.* **2009**, *86*, 1321–1324. [[CrossRef](#)]
62. Myrstad, T.; Fredriksen, G.R. Removal of Fe(CO)₅ from CO gas as detected by FTIR spectroscopy. *Chem. Eng. Technol.* **1998**, *21*, 297–299. [[CrossRef](#)]
63. Williams, T.C.; Shaddix, C.R. Contamination of carbon monoxide with metal carbonyls: Implications for combustion research. *Combust. Sci. Technol.* **2007**, *179*, 1225–1230. [[CrossRef](#)]
64. Carlton, H.E.; Oxley, J.H. Kinetics of the heterogeneous decomposition of iron pentacarbonyl. *AIChE J.* **1965**, *11*, 79–84. [[CrossRef](#)]
65. Poliakoff, M.; Weitz, E. Shedding Light on Organometallic Reactions: The Characterization of Fe(CO)₄, a Prototypical Reaction Intermediate. *Acc. Chem. Res.* **1987**, *20*, 408–414. [[CrossRef](#)]
66. van Leeuwen, P.W.N.M. *Homogeneous Catalysis*; Springer: Cham, The Netherlands, 2004; Volume 3, ISBN 9781461329602.
67. Herrick, D.E.; Tierney, J.W.; Wender, I.; Huffman, G.P.; Huggins, F.E. Activity and Characterization of Coprocessing Catalysts Produced from an Iron Pentacarbonyl Precursor. *Energy Fuels* **1990**, *4*, 231–236. [[CrossRef](#)]
68. Smith, T.W.; Wychlck, D. Colloidal iron dispersions prepared via the polymer-catalyzed decomposition of iron pentacarbonyl. *J. Phys. Chem.* **1980**, *84*, 1621–1629. [[CrossRef](#)]
69. Davidson, J.L. ChemInform Abstract: Homogeneous Catalysis. *Chemischer Informationsdienst* **1978**, *9*. [[CrossRef](#)]
70. King, A.D.; King, R.B.; Yang, D.B. Homogeneous Catalysis of the Water Gas Shift Reaction Using Iron Pentacarbonyl. *J. Am. Chem. Soc.* **1980**, *102*, 1028–1032. [[CrossRef](#)]

71. Pignatello, J.J.; Oliveros, E.; MacKay, A. Advanced oxidation processes for organic contaminant destruction based on the fenton reaction and related chemistry. *Crit. Rev. Environ. Sci. Technol.* **2006**, *36*, 1–84. [[CrossRef](#)]
72. George, S.C.; Thomas, S. Transport phenomena through polymeric systems. *Prog. Polym. Sci.* **2001**, *26*, 985–1017. [[CrossRef](#)]
73. Faupel, F.; Thran, A.; Kiene, M.; Strunskus, T.; Zaporojtchenko, V.; Behnke, K. Diffusion Of Metals In Polymers And During Metal/Polymer Interface Formation. In *Low Dielectric Constant Materials for IC Applications*; Springer: Berlin/Heidelberg, Germany, 2003; pp. 221–251.
74. Faupel, F.; Willecke, R.; Thran, A. Diffusion of metals in polymers. *Mater. Sci. Eng. R Rep.* **1998**, *22*, 1–55. [[CrossRef](#)]
75. Sonnenberg, M.; Gustus, R.; Sedelmeier, S.; Wegewitz, L.; Höfft, O.; Wieser, J.; Maus-Friedrichs, W. Polymer-induced metal diffusion during plastic processing: A reason for deposit formation. *J. Polym. Eng.* **2019**, *39*, 472–480. [[CrossRef](#)]
76. Hordy, N.; Coulombe, S.; Meunier, J.L. Plasma functionalization of carbon nanotubes for the synthesis of stable aqueous nanofluids and poly(vinyl alcohol) nanocomposites. *Plasma Process. Polym.* **2013**, *10*, 110–118. [[CrossRef](#)]
77. Baddour, C.E.; Fadlallah, F.; Nasuhoglu, D.; Mitra, R.; Vandsburger, L.; Meunier, J.L. A simple thermal CVD method for carbon nanotube synthesis on stainless steel 304 without the addition of an external catalyst. *Carbon N. Y.* **2009**, *47*, 313–318. [[CrossRef](#)]



© 2020 by the authors. Licensee MDPI, Basel, Switzerland. This article is an open access article distributed under the terms and conditions of the Creative Commons Attribution (CC BY) license (<http://creativecommons.org/licenses/by/4.0/>).